Lipidomic study of intracellular Singapore grouper iridovirus

Jinlu Wu [a,*], Robin Chan [b,1], Markus R. Wenk [b], Choy-Leong Hew [a]

[a] Department of Biological Sciences, Faculty of Science, National University of Singapore, Singapore 117543, Singapore
[b] Department of Biochemistry, Yong Loo Lin School of Medicine, National University of Singapore, Singapore 117597, Singapore

ARTICLE INFO

ABSTRACT

Singapore grouper iridoviruses (SGIV) infected grouper cells release few enveloped extracellular viruses by budding and many unenveloped intracellular viruses following cell lysis. The lipid composition and function of such unenveloped intracellular viruses remain unknown. Detergent treatment of the intracellular viruses triggered the loss of viral lipids, capsid proteins and infectivity. Enzymatic digestion of the viral lipids with phospholipases and sphingomyelinase retained the viral capsid proteins but reduced infectivity. Over 220 lipid species were identified and quantified from the viruses and its producer cells by electrospray ionization mass spectrometry. Ten caspid proteins that dissociated from the viruses following the detergent treatments were identified by MALDI-TOF/TOF-MS/MS. Five of them were demonstrated to be lipid-binding proteins. This is the first research detailing the lipidome and lipid–protein interactions of an unenveloped virus. The identified lipid species and lipid-binding proteins will facilitate further studies of the viral assembly, egress and entry.

Introduction

Lipids play crucial roles at various stages of host–virus interactions from the virus entry to intracellular trafficking and virus release (Chew et al., 1994; Marsh and Helenius, 2006; Wenk, 2006). Viruses acquire and enrich specific classes of lipids into their envelope structures to increase their infectivity (Brügger et al., 2006; Choi et al., 2005; Mercer and Helenius, 2008). Selective depletion of one lipid class from enveloped viruses can reduce viral infectivity (Goluszko and Nowicki, 2005). On the other hand, compositional changes of cellular lipids are implicated in cell proliferation, apoptosis, stress and viral infection (Bravo et al., 2005; German et al., 2007; van Meer et al., 2008; Vukelic and Kalanj-Bognar, 2001; Wenk, 2006). However, in comparison to many extensive studies of genomes and proteomes, lipidomic studies of viruses and their producer cells are limited and primarily focused on mammalian enveloped viruses (Brügger et al., 2006; Choi et al., 2005; McSharry and Wagner, 1971; Mercer and Helenius, 2008; Schlesinger et al., 1973).

Iridoviruses infect invertebrates mainly insects and poikilothermic vertebrates, such as fish, amphibians and reptiles, and cause systematic diseases. So far, the genomes of twelve iridoviruses have been sequenced (Eaton et al., 2007; Williams et al., 2005). Preliminary studies on the lipid composition of a few iridoviruses, such as frog virus 3 (Willis and Granoff, 1974) and invertebrate iridescent virus 6

(Balange-Orange and Devauchelle, 1982), have been performed by thin-layer chromatography (TLC), but detailed analyses of lipid composition have not been carried out.

Singapore grouper iridovirus (SGIV) infects a number of economically important fishes and replicates in the cytoplasm of infected cells (Qin et al., 2001). The virus has been observed to bud through a plasma membrane (termed extracellular virus), but a majority of newly matured progeny virions accumulate within the cytoplasm as large paracrystalline arrays and are released by cell lysis (termed intracellular virus). Intriguingly, the intracellular viruses are infectious and the viral capsids are coated with a thick layer, whose origin, structure, composition and role remain elusive.

We have previously conducted genomic and proteomic studies on SGIV (Song et al., 2004, 2006). This lipidomic study on the precise composition of SGIV lipids provides complementary information, which is necessary for understanding the viral lipid–protein interaction, entry process, intracellular trafficking, assembly and egress. A combined approach of liquid chromatography and mass spectrometry was used to quantitatively analyze the lipid composition of intracellular SGIV and a grouper embryonic cell (GEC) line in which SGIV replicated. Compared with traditional TLC methods, this analytical approach provides highly selective, sensitive and quantitative determination of lipid molecules in a mixture (Guan et al., 2006; Schwudke et al., 2007). More than 220 species of lipid molecules were measured. We found that the lipid composition of SGIV is significantly different from that of other viruses reported. In addition, ten viral capsid proteins were identified by MALDI-TOF/TOF MS/MS and five of them were confirmed to be lipid-binding proteins. We demonstrated that viral lipids are important for viral integrity and infectivity.

* Corresponding author. Fax: +65 6779 5671.
  E-mail address: dbswjl@nus.edu.sg (J. Wu).
[1] Present address: Columbia University Medical Center, Department of Pathology and Cell Biology, Taub Institute for Research on Alzheimer's Disease and the Aging Brain, 630 W 168th Street P&S 12-510 New York, NY 10032, USA.

Results and discussion

Virus purification

Approximately 80–90% of GECs became detached at day 3 after the infection with SGIV at an MOI of 0.5. The cells were harvested to purify intracellular SGIV by two-step density gradient centrifugation using an iodixanol medium. Iodixanol has been used to purify HIV (Brügger et al., 2006), lipid rafts (Campbell et al., 2004) and subcellular organelles (Choi et al., 2005) for lipid analyses. Purified SGIV pellet displayed green iridescence, indicating that viral integrity was well preserved during the purification. Electron microscopy also showed that the intracellular viral particles were homogeneous (Supplementary data, Fig. S1).

Electron microscopy clearly revealed that the viral capsids were coated with an outer layer before (Fig. 1a) and after (Figs. 1b and c) purification, but an internal lipid membrane, supposed to locate beneath the capsid shell and to be a common structure among iridoviruses, was not observed in our preparation. A high resolution picture from cryo-EM may help to reveal such membrane structure as it was observed in Chilo iridescent virus (Yan et al., 2009). The outer layer of SGIV was much thicker than a common viral envelope which is typically of 5–8 nm thickness. In addition, there was no visible gap between the SGIV outer layer and capsid shell. These observations suggest that the outmost layer may closely interact with the capsid shell and differs significantly from the typical envelope structure of other viruses.

Western blotting showed that the relative amount of actin in the purified viruses had decreased gradually with each step of purification (Fig. 1f). After the final purification step, the actin could not be detected in the viral preparation. This result, together with EM observations, suggests that contamination from cell debris, if present in purified viruses, was below the level of our detection methods.

The lipid characteristics of the viral outer layer

Iridoviruses can be released from their producer cells by budding from a plasma membrane or following whole cell lysis. Regarding SGIV, a majority of viral particles were released from infected cells following cell lysis. To characterize the chemical features of the outer layer of intracellular SGIV, purified particles were treated with ether and DDM. After the treatment with 75% ether, the outer layer became less dense and distorted (Fig. 1d). Treatment with 0.4 mM DDM removed the outer layer (Fig. 1e), but the capsid shell was retained, and viral particles became round. We also observed that the morphology of the viral particles was completely damaged after 50% (v/v) chloroform treatment (data not shown). Overall our data suggest that the outer layer of intracellular SGIV particles might contain lipids that are important in maintaining the viral structure.

High abundance of glycerophosphatidylinositol (PI) in SGIV

To gain an overall understanding of viral lipid composition, lipid extracts from the intracellular SGIV were first analyzed in both negative and positive single stage modes via HPLC-ESI-MS. Prominent peaks in the spectrum of purified SGIV were PI and PS peaks in the negative ionization mode (Supplementary data, Fig. S2a), and the major detected phospholipids in positive mode were PCs (Supplementary data, Fig. S2b). As one control for virus purity, mimic-production from mock-infected cells was subjected to the same procedure, no lipid signal was detectable (data not shown).

In order to obtain a more quantitative description of the lipid inventories of SGIV, the lipid extracts in three independent experiments were then analyzed using MRM, which was optimized to detect only specified ions of interest, thus increasing sensitivity and selectivity of detection, without being affected by the different chemistries of the samples. When normalized to appropriate internal standards, individual classes of lipids (and their individual members) can be presented as a molar percentage of total lipids (Guan et al., 2006). The results are summarized in Table 1 and Supplementary data Fig. S3. The major phospholipid components of SGIV consisted of PC, ePC, PI and SM (Table 1). The molar ratios of PI (18.85 ± 0.98) were higher than those of PE (2.28 ± 0.51), pPE (4.25 ± 1.51) and PS (1.97 ± 0.45). This high proportion of PI in SGIV is distinctive from its relative abundance in reported mammalian viruses, in which the molar ratio of PI was greatly lower than those of PE, pPE and PS (Brügger et al., 2006; McSharry and London, 1971; Schlesinger et al., 1973). The relative high proportion of
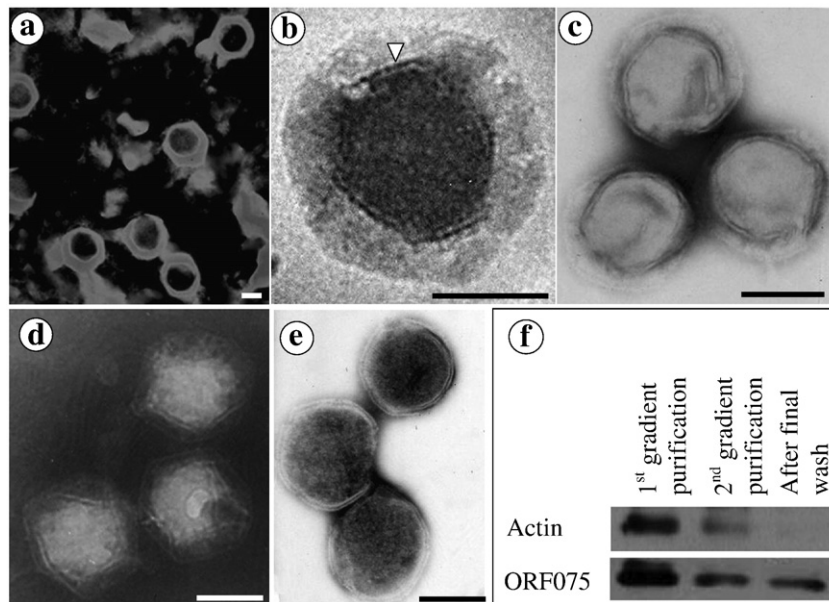

Fig. 1. Electron micrographs of intracellular SGIV particles. (a) Intracellular viral particles observed before purification; (b) and (c) viral particles were purified from cell pellet collected at 3 days after infection by self-generated iodixanol gradients. The layer depicted by an arrow head in (b) is the viral capsid shell. (d) Viral particles after 75% ether treatment; (e) viral particles after 0.4 mM *n*-dodecyl-α-ᴅ maltoside treatment. All those viral preparations were stained with 1% phosphotungstic acid followed by examination under a transmission electron microscope (JEOL 100 CXII). (f) Western blotting analyzed host cellular protein actin and viral structure protein ORF075, showing the amount of actin in purified viruses decreased with each step of purification (bar = 100 nm).

Table 1
Lipid composition of grouper embryonic cells and SGIV.

Lipid class	Uninfected day 1 (mol% ± SD)	Uninfected day 3 (mol% ± SD)	Infected day 1 (mol% ± SD)	Infected day 3 (mol% ± SD)	SGIV (mol% ± SD)
PS	3.85 ± 0.31	3.99 ± 0.33	3.59 ± 0.48	3.72 ± 0.15	1.97 ± 0.45**
PI	10.53 ± 2.62	15.87 ± 0.66*	10.58 ± 0.48*	14.23 ± 0.54	18.85 ± 0.98*
PE	4.04 ± 0.27	3.35 ± 0.20	3.21 ± 0.30*	2.83 ± 0.10**	2.28 ± 0.51*
pPE	9.35 ± 0.58	8.98 ± 0.27	7.84 ± 0.71*	8.16 ± 0.21	4.25 ± 1.51**
PC	29.25 ± 1.44	25.10 ± 3.34	25.24 ± 2.87	28.93 ± 4.94	32.42 ± 1.26*
ePC	9.34 ± 0.73	22.79 ± 3.87**	21.80 ± 2.07	19.75 ± 3.28**	16.78 ± 4.73
Ceramide	4.26 ± 0.12	3.62 ± 0.14**	3.77 ± 0.15	5.38 ± 0.69*	3.42 ± 0.78
MH	13.06 ± 0.29	3.98 ± 0.21**	9.47 ± 0.43	4.56 ± 0.66*	4.08 ± 1.12
DH	2.90 ± 0.38	1.17 ± 0.14**	1.96 ± 0.23	1.35 ± 0.22	1.98 ± 0.36*
SM	10.50 ± 0.38	9.34 ± 0.78	10.21 ± 0.48	9.46 ± 0.85	11.62 ± 2.69
DHSM	2.93 ± 0.24	1.82 ± 0.15**	2.32 ± 0.16	1.61 ± 0.12	2.35 ± 0.59
Chol/PC ratio	0.021 ± 0.003	0.025 ± 0.001	0.024 ± 0.017	0.022 ± 0.004	0.051 ± 0.013

Phospholipid and sphingolipid values are expressed as molar percentages calculated from the absolute signal intensity obtained during Multiple Reactions Monitoring described in Materials and methods. Cholesterol levels are obtained from LC-MS q1 scans in the positive ionization mode and are expressed as a normalized value to total PC levels. Values are the mean ± SD of triplicate experiments each analyzed in triplicate. Significance of the differences was examined with the two-tailed Student's *t*-test at the 0.05 (represented by one asterisk) or 0.01 (represented by two asterisks) level. Paired comparisons of lipid compositions were carried out between samples of SGIV and uninfected day 1; infected and uninfected on day 1; infected and uninfected on day 3 as well as uninfected day 1 and day 3. The abbreviations used are: PS, glycerophosphatidylserine; PI, glycerophosphatidylinositol; PE, phosphatidylethanolamine; pPE, plasmalogen phosphatidylethanolamine; PC, Glycerophosphatidylcholine; ePC, ether phosphatidylcholine; MH, monohexosyl-ceramide; DH, dihexosyl-ceramide; SM, sphingomyelin; DHSM, dihydrosphingomyelin; Chol, cholesterol.

PI was also observed in an iridescent virus type 6 analyzed by TLC (Balange-Orange and Devauchelle, 1982) and other invertebrate iridescent viruses analyzed by gas-liquid chromatography (Williams and Thompson, 1995), suggesting that the high abundance of PI might be a common feature of iridoviruses. Among the invertebrate iridoviruses, the major fatty acids were C18:1 and C16:0, taking approximate 50% of total fatty acids. However, the three most abundant PI species of SGIV were PI 36:2, -38:3 and -38:4, representing a total of 56% of 18 PI species measured (Supplementary Fig. S3), which were different from the fatty acid contents of invertebrate iridoviruses.

Since PIP and PIP2 are involved in many intracellular regulatory processes (Barrero-Villar et al., 2008) and endocytosis (Sun et al., 2007), we further quantified the amount of phosphoinositides (PIPn) in the viruses and GECs. The abundance of both PIP and PIP2 were significantly lower in SGIV compared to that of GECs (Fig. 2), unlike their enrichment reported in retrovirus envelopes (Chan et al., 2008). The Chol/PC ratio of SGIV was higher than that of GECs. It was believed that higher molar ratio of Chol may help stabilization of viral lipid layer in mammalian viruses (Laliberte et al., 2007; Megha and London, 2004). In addition, the coexistence of the two forms of infectious viruses, namely extracellular and intracellular viruses, was observed and intensively studied in rabies viruses (Schlesinger et al., 1973) and vaccinia viruses (Mercer and Helenius, 2008; Roberts and Smith, 2008). However, we failed to isolate such enveloped extracellular viruses despite enormous efforts including using classical sucrose and potassium tartrate gradients. The enveloped viruses were only observed occasionally by electron micrography of ultrathin sections of infected cells (Chew et al., 1994; Qin et al., 2001). It reaffirmed that SGIV infection produces the two forms of mature virions, but a vast majority are the intracellular virions.
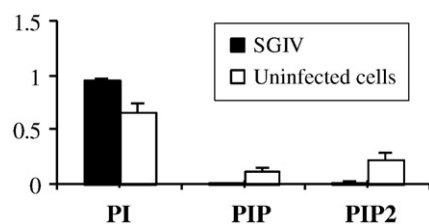

Fig. 2. Abundance of phosphoinostides (PIPn). Phosphoinostides enriched lipid samples were extracted in the acidic condition and quantified as described in Materials and methods. The total amount of PI, PIP and PIP2 was set at one. Bar graph shows relative abundance of glycerophosphatidylinositol (PI), glycerophosphatidylinositol phosphate (PIP) and glycerophosphatidylinositol biphosphate (PIP2) in SGIV and its host cells. All data are mean ± standard deviation (n = 3).

PI and other lipids are mainly synthesized in the endoplasmic reticulum. It has been found that ER membrane contains a relatively higher abundance of PI than other cellular compartment in both mammal and yeast cells (van Meer et al., 2008). Moreover, PI is reported to locate in the inner leaflet of the bilayer in most cell types (Calderón and DeVries, 1997). Analysis of lipid composition of ER of SGIV producer cells may improve our understanding of how SGIV acquires its lipid components.

The role of viral lipids in maintaining viral infectivity

The viral lipids were depleted using one solvent (ether), three detergents and three lipases to examine their effects on viral infectivity. The treatments with 75% ether and 0.1% Triton X-100 caused the virus titers to drop approximately two logarithms losing more than 98% of viral infectivity (Fig. 3a). OG and DDM are mild detergents and commonly used in protein crystallization to improve protein solubility while retaining proteins in their natural conformations. Treatment with 0.4 mM DDM abolished viral infectivity by 99.99%, a drop of viral titer from $10^{6.54}$ to $10^{2.54}$. However, OG seemed less effective in reducing infectivity when it was used at the same concentration as DDM. Treatment with 0.4 mM OG reduced infectivity by just 30%. Interestingly, it was reported that disruption of the lipid bilayer in invertebrate iridescent viruses had a profound effect on their ability to infect cultured cells but not to infect whole insects when the virus was injected into the haemocoel (Martinez et al., 2003), suggesting that viruses may take different routes to establish an infection *in vivo* from *in vitro*. On the other hand, restoration of viral lipids with liposomes prepared from GECs increased the infectivity of DDM-treated virus by three-fold (Fig. 3b).

To further explore the viral lipid characteristics, we performed enzymatic digestion of intact viruses with PLA2, PLC and Smase. PLA2 hydrolyzes phospholipids at the sn-2 position to form fatty acid and lysophospholipid products. PLC hydrolyzes phosphatidylinositol to yield diacylglycerol and a phosphate-containing head group, whereas Smase hydrolyzes SM yielding ceramide and phosphocholine. The perturbation of viral lipids by PLC, Smase as well as a combination treatment with the two enzymes slightly affected viral infectivity, leading to a reduction of infectivity by 18%, 22% and 35%, respectively. However, the PLA2 treatment resulted in a drop of 96% of infectivity compared with mock-treated viruses (Fig. 3c). PLA2 treatment resulted in a similar effect on the frog virus 3 (FV3) (Willis and Granoff, 1974), but no effect on invertebrate iridescent viruses (Martinez et al., 2003), which hint that the composition and role of phospholipids may differ between vertebrate and invertebrate iridoviruses.
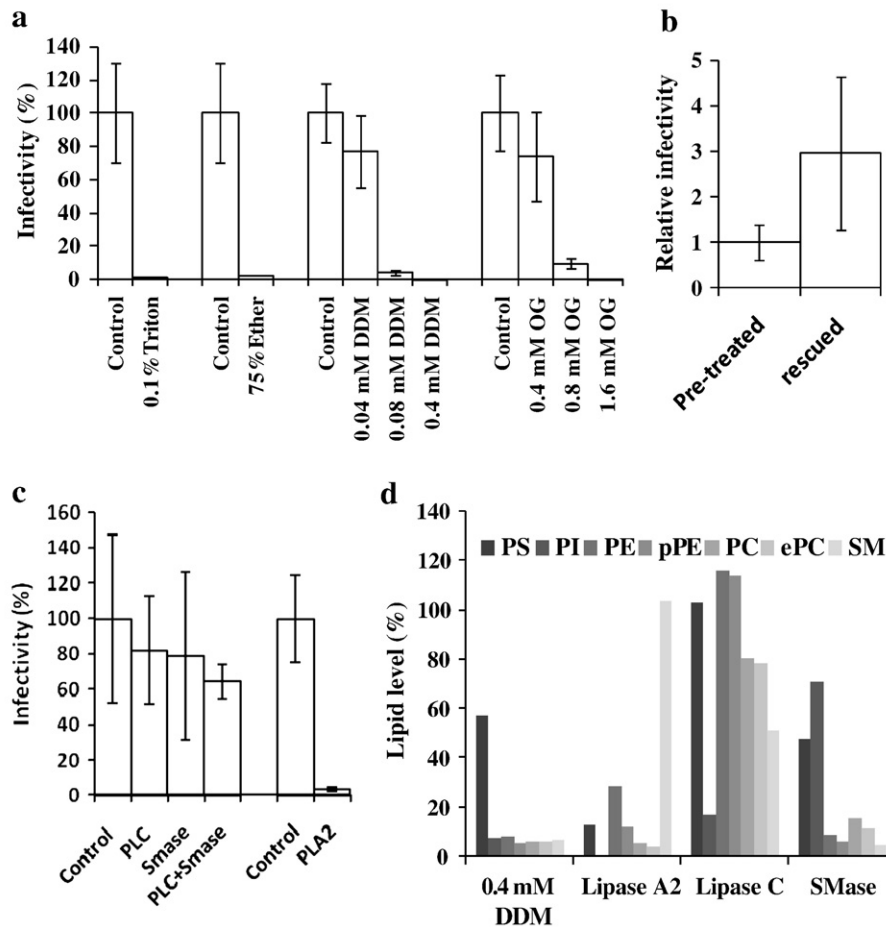
Fig. 3. Effects of solvent, detergent and lipase treatments on viral lipid composition and viral infectivity. Viral infectivity was determined by TCID$_{50}$ assay. The data represents the means of three independent experiments. Error bars represent standard deviation of the mean. (a) Viruses were treated with Triton, ether, *n*-dodecyl-α-ᴅ maltoside (DDM) and *n*-octyl-β-ᴅ-glucopyranoside (OG). Viral infectivity is expressed as the percentages of the untreated control. (b) Pre-treated intracellular viruses with 0.2 mM DDM were incubated with liposome prepared from host cell lipids to rescue viral infectivity. The rescued viruses show a 3-fold higher infectivity than the pre-treated ones. (c) Viruses were treated with phospholipase C (PLC), phospholipase A2 (PLA2) and sphingomyelinase (Smase). Viral infectivity is expressed as the percentages of the untreated control. (d) Depletion of viral lipids by various treatments was quantitatively analyzed as described in Materials and methods. The abundance of each lipid group in treated viruses is shown as the percentage of the corresponding lipid group in untreated control, which was set to 100.

The lipid contents of enveloped viruses are usually crucial for infectivity. Our results indicate that the lipids in a non-typically enveloped virus are also important for maintaining infectivity. Nevertheless, viruses without an envelope structure may capture some lipids on its surface that enhance its infectivity. Studies of human viruses indicated that viral entry involves single lipid species and lipid raft (Laliberte and Moss, 2009; Marsh and Helenius, 2006). A study of FV3, a prototype of Ranavirus, proposed that the enveloped viral particle were internalized by endocytosis, while uneveloped particles entered the host cells by fusion between the virus shell and the cellular membranes (Braunwald et al., 1985). For SGIV, our hypothesis is that lipids in the outer layer of intracellular viruses may facilitate the viral particles to bind to cellular membrane and subsequent fusion with plasma membrane, while the viral internal lipid membrane may facilitate uptake by the intracellular organelles.

Alteration of the viral lipid and protein compositions after detergent and lipase treatments

To understand the underlying causes of the loss of viral infectivity and symmetrical morphology, we continued to investigate the compositional changes of viral lipids and proteins following each of the treatments. Treatment of SGIV with 0.4 mM DDM triggered a more than 90% loss of most lipids except for PS, which was only reduced by 42% (Fig. 2d). Treatment with LPA2 resulted in a general hydrolysis of

phospholipids, and SM was retained in the virus. When SGIV was incubated with PLC, PI was specficially hydrolyzed and other lipids did not seem to be affected. However, the treatment with SMase resulted in the removal of SM species as well as other phospholipids. These results suggest that SM and phospholipids may be arranged so that phospholipids are situated in the outer surface of the viral outer layer or that SM may link to other viral components such as capsid proteins. On the other hand, PI, which was found to be in a higher abundance than many other lipids, did not appear to have such an interconnection with other lipids since its loss was specific.

The examination of the protein profiles of DDM-treated viruses by SDS-PAGE revealed that several viral proteins were partially dissociated from viral particles and moved into the supernatant after centrifugation (Supplementary data Fig. S4). A total of ten proteins were identified by MS/MS (Table 2). ORF075 was one of the abundant structure proteins (Song et al., 2006), showing an obvious reduction in treated viral particles (Supplementary Fig S4a). ORF52L and ORF60R with a predicted molecular mass of 109 kDa were identified from the gel bands at a migration distance equivalent to a 40-kDa entity. This result indicated that these two proteins might be fragmented by 0.4 mM DDM treatment and migrated faster during SDS-PAGE. The protein peptides corresponding to these proteins were therefore identified from the location of 40 kDa entity. Proteins listed in Table 2 are promising targets for identification of lipid binding proteins and viral surface proteins. In contrast, enzyme treatments did

Table 2
Dissociated viral proteins from SGIV particles detected by MALDI-TOF/TOF MS/MS after detergent treatments.

Band no.	ORF	MW, kDa	PI	Best-matched peptide	Predicted function (p-value %)/motif scan
1/6	**ORF90L**	43	7.74	DYWFSLGYDNVHVLSVANR	Lipid-binding proteins (90)/none
2/8/10	ORF72R	50.5	6.31	VSGNPAFGQEFSVGVPR	Major coat protein (98)/MCP
2	**ORF101R**	35	6.11	AVPHDEVPNFR	Transmembrane (98)/none
3/12	**ORF75R**	20	4.50	ILAHGELLPNER	Zinc-binding (62) /none
4	ORF69L	61.9	9.62	MALTLAPLQTDVSVNEVR	Iron-binding (99) /none
5	**ORF26R**	63.3	6.38	GAAVQTGENTGFSEMTIR	Carbon lyases (94) /none
6	ORF52L	109.9	7.67	TAFGDMALPESWGRPTSDR	Iron-binding (97)/helicase
7	**ORF89L**	45.6	8.13	QEILELGLDINER	Iron-binding (91) /none
9	ORF60R	109.7	8.97	SVQAEGINTYNSLFR	Zinc-binding (98)/ NTPase
11	ORF18R	32.3	6.01	ATAVEAVLKPR	Zinc-binding (96) /none

Proteins in bold letters were confirmed to be lipid-binding proteins. Function was predicted using online software: http://jing.cz3.nus.edu.sg/cgi-bin/svmprot.cgi and http://www.ebi.ac.uk/InterProScan/.

not cause obvious changes in viral protein profiles examined by SDS-PAGE or obvious changes in viral morphology by EM observation (data not shown).

Taken together, although both lipase and detergent treatments reduced viral infectivity in our experimental conditions; DDM (0.4 mM) triggered a more serious loss of infectivity than did the lipases. This may be because the DDM treatment leaded to the dissociation of both lipids and proteins from the viral particles, whereas the lipase treatments only depleted certain lipids from the viral particles. Selective depletion of enriched viral lipids did result in the reduction of infectivity, but that reduction was limited. It is interesting to note that the conformation of proteins that play a role in membrane fusion during viral entry is affected by surrounding lipids in HIV, influenza virus and SARS coronavirus (Qiang and Weliky, 2009, Guillén et al., 2008). When the fusion peptide (FP, the N-terminal domain of HIV-1 gp41) was associated with cholesterol-containing membranes, the FP correlated with beta strand conformation while association with membranes without cholesterol resulted in a

mixture of helical and beta strand conformations. Studies of SARS FP revealed that the peptide organization is different depending if it is in water or bound to the membrane. Our results hint at the cooperation roles of viral lipids and proteins in the viral infectivity. The association of lipids and viral capsid proteins may be involved in the merging of the viral external layer and target cell membranes.

Lipid–protein interactions

SDS-PAGE analysis showed a clear band of each purified recombinant protein (Fig. 4a), and they were recognized by the corresponding antibody via Western blotting (Fig. 4b). The analysis of lipid–protein interaction using PIP strips revealed that ORF26R, 75R, 89L, 90L, and 101R were bound to different lipid species (Fig. 5), whereas ORF18R and ORF158L were not (data not shown). Each lipid-binding protein showed a different affinity to different lipid species, so that each protein may contribute differently to the overall complexity of viral lipids. It has been demonstrated that PIP2 is involved in viral entry process and replication in HIV (Barrero-Vilar et al., 2008) and influenza viruses (Ehrhardt and Ludwig et al., 2009). Although PIP and PIP2 were not enriched in the intracellular SGIV (Fig. 3), it was obvious that ORF75R bound specifically to PIP and PIP2, while ORF90L and 101R bound to PI in addition to PIP2. A study on a lipid binding protein ORF-9b from the SARS coronavirus revealed that lipid binding was important for intracellular trafficking of the protein and viral assembly (Meier et al., 2006). This analysis demonstrated that SGIV structural proteins have the capacity to acquire specific lipid species, which may function in intracellular trafficking of the proteins and viral assembly.

Lipid profiles of infected and uninfected cells

To examine the impact of SGIV infection on host lipid metabolism, we performed quantitative analysis of SGIV-infected and uninfected GECs sampled over three consecutive days (Fig. 3S). Unexpectedly, we
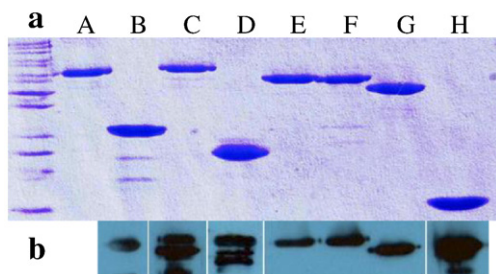

Fig. 4. SDS-PAGE analysis and Western blot detection of purified recombinant proteins. Lane A, bovine serum albumin (BSA); lane B–H, recombinant proteins of ORF18R, 26R, 75R, 89L, 90L, 101R, and 158L. Two microgram of BSA was loaded on the gel to provide a reference for protein quantification. All purified recombinant proteins show a clear major band (4a) and could be detected by the corresponding antibodies (4b).
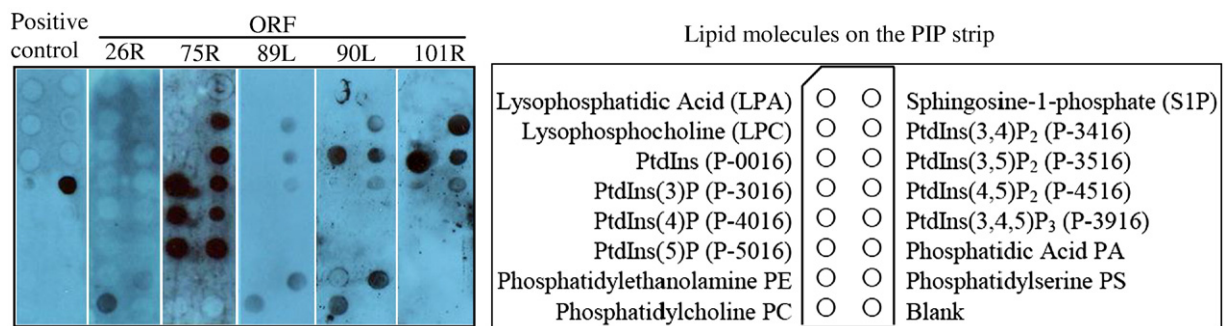

Fig. 5. Lipid–protein interaction assay. 0.01 mM of each viral protein was incubated with PIP-Strips (echelon), showing their binding abilities to the different lipid molecules (right). The first strip was a positive control using one μg/ml PIP2 Grip™ protein. ORF18R and -158L did not show binding affinity to the lipids (data not shown). A diagram in the left shows lipid molecules on the PIP strip. PtdIns represents phosphatidylinositol.
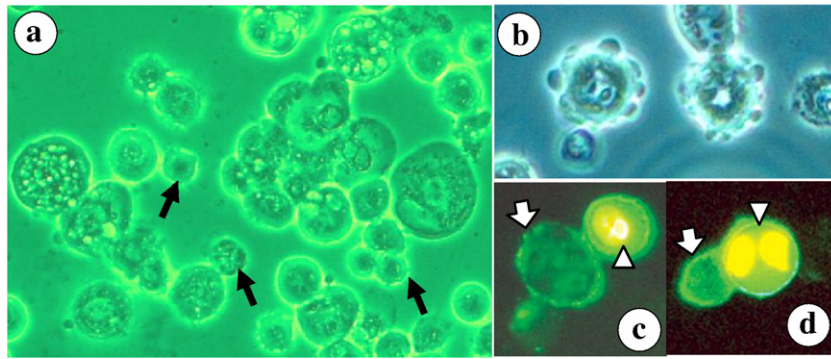
Fig. 6. Apoptosis induced by SGIV infection. Light micrographs of SGIV infected cells show cell shrinkage (a, solid arrows) and apoptotic bodies (b). Fluorescent microscopic analysis of apoptotic cells stained with FITC annexin V/propidium iodide (c and d). Apoptotic cells are denoted by open arrows while dead or necrotic cells are denoted by arrow heads. Necrotic cell nuclei permitted staining propidium iodide.

observed that lipid profiles of uninfected GECs changed over time. The molar ratios of PI and ePC increased, while those of Cer, MH, DH and dihydrosphingomyelin (DHSM) decreased from day 1 to day 3. The increase in PI was mainly attributed to PI -36:1, -36:0 and -38:1, whereas the increase in ePC showed a distinct pattern, i.e., all measured saturated and monounsaturated ePC molecules increased, but polyunsaturated species did not. In contrast, the overall abundance of sphingolipids decreased over the 3 days (Table 1 and Supplementary Table S1, Supplementary Fig. S3). A previous study on human skin fibroblasts has revealed that lipid biosynthesis might be involved in the regulation of cell growth and is dependent on cell density (Vukelic and Kalanj-Bognar, 2001). The changes in the uninfected GEC lipids may be triggered by similar factors, including alterations in cell density, nutrients and medium pH values.

Due to the changes of uninfected GEC lipids over time, better understanding of host cell lipid dynamics in the context of virus infection will require further bioinformatics analysis and/or experimental investigations. Nevertheless, we present here an analysis of those changes, which might be related to apoptosis, to highlight the importance of further study of these lipids. Several members in the Iridoviridae can induce apoptosis during infection (Chinchar et al., 2003; Chitnis et al., 2008; Huang et al., 2007; Imajoh et al., 2004), but apoptosis caused by SGIV infection has not been reported previously. Morphological changes of SGIV-infected cells related to apoptosis, such as cell shrinkage (Fig. 6a) and apoptotic body-like blebbing (Fig. 6b) were observed. PS translocation to the cell surface, as a marker of early-stage apoptosis, was also detected in SGIV-infected GECs by Annexin-V labeling (Figs. 6c and d) for the first time in this study.

It is well documented that high levels of ceramide usually promote apoptosis through an intrinsic apoptotic pathway (Reynolds et al., 2004; Thevissen et al., 2006). Our results revealed that the relative amounts of ceramide in infected cells increased from 0.9 to 1.2 and 1.5 fold compared to mock infected cells at 1 dpi, 2 dpi and 3 dpi, respectively. This suggests that increased ceramide might be a factor causing apoptosis in SGIV-infected cells. In addition, a closer comparison of lipid profiles of infected and uninfected cells measured at day 1 revealed significant decreases of PE ($p<0.01$) and MH ($p<0.05$) as well as a slight decrease of PC (Table 1). Concurrently, SGIV infection significantly increased the molar ratio of ePC ($p<0.01$) at day 1. Previous studies of the apoptosis of hematopoietic progenitor cells found a decrease of PE and PC and a concomitant increase of ePC (Fuchs et al., 2007.), which is similar to our observation in SGIV-infected GECs. These results provide an insight into the possible relationship between apoptosis and metabolic changes of lipids in SGIV-infected cells for the first time.

In summary, we identified more than 220 species of lipid molecules in 12 lipid groups from the purified intracellular unenveloped SGIV and grouper embryonic cells (Supplementary Fig. S3). Depletion of the

viral lipids by detergents and lipases resulted in the loss of the viral proteins, integrity, and infectivity. This is the first quantitative analysis of the lipidomes of a fish virus and a fish cell line. The lipid database will be useful for comparative study with other types of viruses and cell lines. Five of the ten identified viral capsid proteins were confirmed to be lipid-binding proteins. The identified lipid molecules and lipid-binding proteins provide a novel resource to investigate viral protein trafficking, assembly, egress and entry mechanisms.

Materials and methods

Reagents

Unless otherwise stated, all reagents were purchased from Sigma. Lipid standards were purchased from Avanti Polar Lipid Inc. or Echelon Biosciences Inc.

Cell culture

Grouper embryonic cells (GECs) from *Epinephelus tauvina* (Chew et al., 1994) were maintained at 26 °C in Eagle's minimum essential medium containing a final concentration of 10% fetal bovine serum, 162 mM NaCl, 5 mM HEPES, 100 IU of penicillin G per ml (GIBCO), 0.1 mg streptomycin sulfate per ml (GIBCO), and adjusted to pH 7.4 with NaHCO$_3$.

Virus infection, sampling and purification

Freshly confluent monolayers of GECs were inoculated with SGIV at a multiplicity of infection (MOI) of approximately 0.5. Infected GECs were detached using cell scrapers and harvested at day 1, day 2 and day 3 post-infection (dpi) by centrifugation at $500 \times g$ for 5 min. Uninfected GECs were collected in parallel with infected GECs as a control. The collected cells were washed twice with ice-cold TNE buffer (50 mM Tris, pH 7.4, 100 mM NaCl and 5 mM EDTA) and subjected to lipid extraction.

At three dpi cell pellets were collected from more than 400 flasks, each with 175 cm^2 cell growth areas, by centrifugation at $500 \times g$ for 5 min, washed twice with cold TNE buffer and then stored in liquid nitrogen. To purify intracellular viral particles, the stored pellets were homogenized in ice-cold TNE buffer to release intracellular SGIV. The homogenate was then layered on a discontinuous gradient formed from equal volumes of 5%, 10%, 20% and 30% (wt/vol) OptiPrep iodixanol. All iodixanol solutions were prepared in a buffer containing 7.4% sucrose, 20 mM Tris, pH7.4 and 2 mM EDTA. The gradients were centrifuged in a Beckman SW28 rotor at $55,000 \times g$ for 1 h at 4 °C. A virus band at the interface between 20% and 30% iodixanol was aspirated and mixed with 25% iodixanol. The mixture

was centrifuged in a Beckman SW41Ti rotor at 87,000×g overnight at 4 °C to form a self-generated continuous gradient to further purify the virus (Ford et al., 1994). A visible virus band was collected and washed twice in TNE buffer by centrifugation. The purity of the virus was examined at each step of purification by transmission electron microscopy (EM) (JEOL 100 CXII) after negative staining, as well as by Western blotting using antibodies of anti-actin (Chemicon, MAB1501R) and anti-SGIV structural protein ORF75R. As another negative control for viral purity, a batch of mock-infected cells was subjected to the same procedures of virus purification, lipid extraction and lipid analysis. For mock-infected samples, an equal volume of substances was collected after centrifugation from the same density region where the virus band located in the viral infected sample.

The lipid features of the viral outer layer

A small portion of purified viruses were divided into two groups. One was incubated with 75% ether (v/v), while the other was incubated with 0.4 mM n-dodecyl-α-ᴅ maltoside (DDM) at 27 °C for 30–60 min. Both groups were then washed with cold TNE buffer by centrifugation to remove the ether and DDM and examined under EM after negative staining.

Sensitivity of SGIV to solvent, detergents and lipases

SGIV preserved in the cell culture medium was aliquoted into small tubes, each was treated at 27 °C for 1 h with one of the following reagents: 75% (v/v) ether; 0.1% (v/v) Triton X-100; different concentrations (0.04, 0.08, and 0.4 mM) of DDM as well as different concentrations (0.4, 0.8 and 1.6 mM) of n-octyl-β-ᴅ-glucopyranoside (OG). After the treatments, the ether and detergents were removed by washing with cell culture medium and centrifugation. One small portion of treated viruses was subjected to TCID50 assay using the Reed-Muench method, whereas the remaining large portion was used for investigating the alteration of viral lipids and proteins. Each of the treatments and TCID50 assays were performed in triplicate.

Enzymatic digestion of intracellular SGIV with phospholipase A2 (PLA2, P9279), phospholipase C (PLC, P8804) and sphingomyelinase (Smase, S9396) was performed as reported previously (Willis and Granoff, 1974). Briefly, approximately 5×10^7 of purified SGIV was incubated with 1 U of each enzyme at 25 °C for 30 min. A combination treatment with 1U PLC and 1U Smase was also carried out in parallel. A mock-treatment of the virus with reaction buffer only was carried out as a control. The enzymatic digestion was terminated by addition of EDTA to a final concentration of 0.2 M and rapid chilling. The viral titer was determined following the same method as for detergent-treated viruses.

To investigate alteration of viral lipids after the treatments, viruses treated with 0.4 mM DDT, LPA2, PLC and Smase were harvested by centrifugation and subjected to lipid extraction and analysis using the same methods described below for untreated SGIV. Every analysis on treated viruses was carried out with a mock-treated (untreated) virus control. The changes of lipid compositions were expressed as percentages calculated by a comparison of the lipid amount of the treated viruses against that of the untreated viruses. To investigate alteration of viral protein profile, the treated viruses were separated into viral pellet and supernatant phases by centrifugation. Proteins in the both phases were examined by SDS-PAGE with mock-treated viruses as a control. The bands depicting the differences in protein abundance between the treated and mock-treated viruses were sliced from the protein gel and identified by MALDI-TOF/TOF MS/MS as described previously (Song et al., 2006). Computational analysis of identified proteins was performed using the online software: http://jing.cz3.nus.edu.sg/cgi-bin/svmprot.cgi and http://www.ebi.ac.uk/InterProScan/.

Interactions of viral proteins and lipids

Ten SGIV genes corresponding to the proteins identified by mass spectrometry were cloned into different several vectors to optimize their expression and solubility, and six of them were successfully expressed in *E. coli*. ORF26R, 89L, 90L, and 101R were inserted into pET28a-SUMO plasmid vector. pET28a-SUMO is a modified plasmid vector of pET28a with an insertion of SUMO gene between restriction digestion sites of NdeI and BamHI. ORF75R and 18R were cloned into pET15b and pGEX6p-1, respectively. In addition, a gene that encodes a non-structural SGIV protein ORF158L was also cloned into pET15b and expressed in *E. coli* as a control to the six viral structural proteins during the lipid–protein binding assay.

His-tagged fusion proteins of ORF26R, 89L, 90L, 101R and 158L were purified under native condition by Ni-NTA affinity beads (Qiagen) following the manufacturer's protocol. The elution fractions from Ni-NTA column underwent further purification by size-exclusion FPLC (GE). His-tagged ORF75R was purified under denaturing conditions by Ni-NTA affinity beads, followed by on-beads refolding in 10 mM Tris–HCl buffer (pH 7.0) at 4 °C for 4 h. Eluted protein was further purified by size-exclusion FPLC (GE). GST-tagged ORF18R was purified with GST 4B beads (GE) and the eluted fraction was further purified by size-exclusion FPLC Superdex75TM (GE).

Lipid–protein interactions were examined using PIP Strips™ (Echelon) which contain 100 pmol per spot of all eight phosphoinositides and other biologically active lipids (Fig. 5). Briefly, the purified viral recombinant proteins were quantified using a Bradford Assay Kit (BioRad). The strip was incubated with 0.01 mM of each viral recombinant protein in PBS + 1% nonfat-dry milk for 1 h at RT and then washed three times with PBS + 0.5% Tween 20. Protein binding to the strip was detected by the corresponding antibody against the protein and visualized by enhanced chemiluminescence reagents (ECL™ detection reagents, Amersham). Anti-rabbit antibodies against ORF18R, 26R, 75R and 158L were produced by us for this purpose. A 6 His tag antibody (Abcam, ab18184) was used for detection of ORF 89L, 90L and 101R. PIP2 Grip™ protein (1 μg/ml) was used as a positive control as recommended by the manufacturer (Echelon Biosciences Inc., UT, USA).

Rescue viral infectivity with liposome

Total lipids extracted from uninfected GECs (described in the next paragraph) were hydrated by adding cell culture medium at a final concentration of 7.5 mg/ml and vortexed vigorously at 27 °C for 1 h to form a milky suspension. The suspension was then sonicated (Vibra-Cells 750 Watt) to form small liposomes. Viruses pretreated with 0.2 mM DDM were divided into two groups, one incubated with the liposomes at 4 °C for 2 h with shaking and the other incubated with cell culture medium as a control. After the incubation, the virus titer was determined by TCID50 using the same procedure as previously described.

Lipid extraction

Three kinds of lipid extracts, namely total lipids (covering most lipids), enriched phosphoinositides (PIPn) and sphingolipids, were prepared as described previously (Bligh and Dyer, 1959; Chan et al., 2008; Merrill et al., 2005) from each of the following samples: purified intact intracellular SGIV; detergent-treated SGIV; lipase-treated SGIV; uninfected GECs harvested at day 1, day 2 and day 3; as well as infected GECs harvested at day 1, day 2 and day 3 post-inoculation.

For total lipid extraction (Bligh and Dyer, 1959), the samples were first spiked with a cocktail of internal standards that included 1,2-dimyristoyl-glycero-phosphoserine (DMPS); 1,2-dimyristoyl-glycero-3-phosphoethanolamine (DMPE); 1,2-dimyristoyl-glycero-3-phosphocholine (DMPC); lauroyl sphingomyelin (L-SM); *N*-heptadecanoyl-

ᴅ-erythro-sphingosine (C17 Cer.) and ᴅ-glucosyl-β1-1′-N-octanoyl-ᴅ-erythro-sphingosine (C8 Glu-Cer.) (Avanti Polar Lipids, Alabaster AL) which allowed the measurement of glycerophosphatidylserine (PS), phosphatidylethanolamine (PE), plasmalogen phosphatidylethanolamine (pPE), glycerophosphatidylcholine (PC) and ether phosphatidylcholine (ePC), sphingomyelin (SM), ceramide (Cer) and glucosylceramide (Glu-Cer), respectively. A volume of 0.6 ml of chloroform/methanol (Chol/Meth, 1:2, v/v) mix was added to the sample before vortexing. This was followed by addition of 0.3 ml Chol and 0.2 ml 1 M KCl and further vortexing. The mixture was then centrifuged for 2 min at 9000 rpm to cause phase separation. The lower organic layer was collected and dried using a speed vacuum.

PIPn enriched lipid samples were prepared by replacing 1 M KCl with 1 M HCl solution and following the same procedure as for total lipid extraction (Chan et al., 2008). Internal standards contained 1,2-dioctanoyl-glycero-3-phosphoinositol (C8-PI), 1,2-dioctanoyl-glycero-3-[phosphoinositol-4-phosphate] (C8-PI (4) P) and 1,2-dioctanoyl-glycero-3-[phosphoinositol-4, 5-bisphosphate] (C8-PI (4, 5) P2).

Sphingolipid samples were prepared by first adding 0.75 ml of Chol/Meth (1:2) followed by incubation overnight at 48 °C (Merrill et al., 2005). Alkaline hydrolysis of glycerophospholipids was carried out by adding 75 µl of 1 M KOH in Meth and incubating for 2 h at 37 °C. The sample was then neutralized with 6 µl of glacial acetic acid. Lastly, 0.5 ml of Chol and 0.3 ml of water were added to the tube. The mixture was then centrifuged for 2 min at 9000 rpm, and the lower organic layer was collected and dried as above. Internal standards contained L-SM, C17-Cer., C8-Glu-Cer., ᴅ-erythro-Sphingosine (C17-sphingosine) and ᴅ-erythro-sphingosine-1-phosphate (C17-sphingosine-1-phosphate).

Lipid composition analysis

Total lipid profiling was performed via electrospray ionization mass spectrometry (ESI-MS) with a triple quadrupole instrument (ABI 4000QT) connected to an upfront HPLC column and Agilent 1100 autosampler-pump setup. Isocratic elution was achieved using Chol/Meth/100 mM ammonium acetate (1:1:2%, v/v/v) at a flow rate of 400 µl/min as a mobile phase. The ion source temperature was set at 300 °C while the declustering potential and collision energy was set at ± 30 eV and ± 10 eV for positive and negative modes, respectively. The mass spectrum was acquired in the negative mode from 400 to 1300 m/z while the positive mode was acquired from 300 to 1300 m/z at a rate of one scan per second for a total of 18 min. Lipids were dissolved in Chol/Meth (1:1, v/v) and 30 µl of the sample was injected for analysis. The spectra data were produced by integrating the chromatogram from about 3 to 16 min. Chol levels were calculated by normalizing the 369 m/z peak intensity against the total PC peak intensity**.** A cholesterol-to-PC molar ratio (Chol/PC ratio) was used to compare the Chol abundance among the samples (Brügger et al., 2006).

For quantitative measurement of lipids, the multiple reactions monitoring (MRM) function of the same instrument without upfront HPLC was used (Wenk et al., 2003). More than 220 lipid species were measured in this method. The total lipid and sphingolipid extracts were dissolved in Chol/Meth (1:1, v/v) and, typically, 10 to 15 µl of samples were injected. For the PIPn samples, the lipids were dissolved in Chol-Meth 1:1, spiked with 10% piperidine solution (300 ng/ml) and injected directly into the mass spectrometer. The signal intensity obtained for each lipid species was converted to its molar equivalent by normalization to the appropriate internal standard. Molar percentage of lipid composition was calculated as described previously (Schlesinger et al., 1973). The standard deviations represent the differences in at least three sets of replicates, i.e., $n \geq 3$. Lipid composition of the SGIV was compared with that of uninfected GECs of the day 1 sample to identify differences. A day-to-day comparison of lipid composition between infected and uninfected GECs was carried out to examine the changes of GEC lipid profiles. The significance of observed differences was determined using the two-tailed Student's *t*-test at the $p = 0.05$ (represented by one asterisk) or 0.01 (represented by two asterisks) levels.

Detection of apoptosis

GECs were grown in four-well Lab-Tek® chambers and infected with intracellular SGIV at an MOI of 0.5. Mock-infected cells served as negative controls. Apoptotic morphological changes were monitored by phase contrast microscopy. Normal viable, apoptotic and necrotic cells were distinguished by Annexin-V labelling and propidium iodide staining using a Vybrant™ Apoptosis Assay Kit (Molecular Probe) according to kit instructions. Slides were mounted with FluorSave™ reagent (Calbiochem) and observed under a Zeiss fluorescence microscope.

Appendix A. Supplementary data

Supplementary data associated with this article can be found, in the online version, at doi:10.1016/j.virol.2010.01.016.

References

Balange-Orange, N., Devauchelle, G., 1982. Lipid composition of an iridescent virus type 6 (CIV). Arch. Virol. 73, 363–367.

Barrero-Villar, M., Barroso-González, J., Cabrero, J.R., Gordón-Alonso, M., Alvarez-Losada, S., Muñoz-Fernández, M.A., Sánchez-Madrid, F., Valenzuela-Fernández, A., 2008. PI4P5-kinase Ialpha is required for efficient HIV-1 entry and infection of T cells. J. Immunol. 181, 6882–6888.

Bligh, E.G., Dyer, W.J., 1959. A rapid method of total lipid extraction and purification. Can. J. Biochem. Physiol. 37, 911–917.

Braunwald, J., Nonnenmacher, H., Tripier-Darcy, F., 1985. Ultrastructural and biochemical study of frog virus 3 uptake by BHK-21 cells. J. Gen. Virol. 66, 283–293.

Bravo, I.G., Crusius, K., Alonso, A., 2005. The E5 protein of the human papillomavirus type 16 modulates composition and dynamics of membrane lipids in keratinocytes. Arch. Virol. 150, 231–246.

Brügger, B., Glass, Haberkant, B.P., Leibrecht, I., Wieland, F.T., Kräusslich, H.G., 2006. The HIV lipidome: a raft with an unusual composition. Proc. Natl. Acad. Sci. U. S. A. 103, 2641–2646.

Calderón, R.O., DeVries, G.H., 1997. Lipid composition and phospholipid asymmetry of membranes from a Schwann cell line. J. Neurosci. Res. 1, 372–380.

Campbell, S., Gaus, K., Bittman, R., Jessup, W., Crowe, S., Mak, J., 2004. The raft-promoting property of virion-associated cholesterol, but not the presence of virion-associated Brij 98 rafts, is a determinant of human immunodeficiency virus type 1 infectivity. J. Virol. 78, 10556–10565.

Chan, R., Uchil, P.D., Jin, J., Shui, G., Ott, D.E., Mothes, W., Wenk, M.R., 2008. Retroviruses HIV and MLV are enriched in phosphoinositides. J. Virol. 82, 11228–11238.

Chew, L.M., Ngoh, G.H., Ng, M.K., Lee, J.M., Chew, P., Li, J., Chan, Y.C., Howe, J.L.C., 1994. Grouper cell line for propagating grouper viruses. Sing. J. Prim. Ind. 22, 113–116.

Chinchar, V.G., Bryan, L., Wang, J., Long, S., Chinchar, G.D., 2003. Induction of apoptosis in frog virus 3-infected cells. Virology 15, 303–312.

Chitnis, N.S., D'Costa, S.M., Paul, E.R., Bilimoria, S.L., 2008. Modulation of iridovirus-induced apoptosis by endocytosis, early expression, JNK, and apical caspase. Virology 370, 333–342.

Choi, K.S., Hideki, A.M., Lai, M.C., 2005. Murine coronavirus requires lipid rafts for virus entry and cell-cell fusion but not for virus release. J. Virol. 79, 9862–9871.

Eaton, H.E., Metcalf, J., Penny, E., Tcherepanov, V., Upton, C., Brunetti, C.R., 2007. Comparative genomic analysis of the family Iridoviridae: re-annotating and defining the core set of iridovirus genes. Virol. J. 4, 11.

Ehrhardt, C., Ludwig, S., 2009. A new player in a deadly game: influenza viruses and the PI3K/Akt signaling pathway. Cell. Microbiol. 11, 863–871.

Ford, T., Graham, J., Rickwood, D., 1994. Iodixanol: a nonionic iso-osmotic centrifugation medium for the formation of self-generated gradients. Anal. Biochem. 220, 360–366.

Fuchs, B., Schiller, J., Cross, M.A., 2007. Apoptosis-associated changes in the glycerophospholipid composition of hematopoietic progenitor cells monitored by 31P NMR spectroscopy and MALDI-TOF mass spectrometry. Chem. Phys. Lipids 150, 229–238.

German, J.B., Gillies, L.A., Smilowitz, J.T., Zivkovic, A.M., Watkins, S.M., 2007. Lipidomics and lipid profiling in metabolomics. Curr. Opin. Lipidol. 18, 66–71.

Goluszko, P., Nowicki, B., 2005. Membrane cholesterol: a crucial molecule affecting interactions of microbial pathogens with mammalian cells. Infect. Immun. 73, 7791–7796.

Guan, X.L., He, X., Ong, W.Y., Yeo, W.K., Shui, G., Wenk, M.R., 2006. Non-targeted profiling of lipids during kainate-induced neuronal injury. FASEB J. 20, 1152–1161.

Guillén, J., de Almeida, R.F., Prieto, M., Villalaín, J., 2008. Structural and dynamic characterization of the interaction of the putative fusion peptide of the S2 SARS-CoV virus protein with lipid membranes. J. Phys. Chem. B. 12 (112), 6997–7007.

Huang, Y.H., Huang, X.H., Gui, J.F., Zhang, Q.Y., 2007. Mitochondrion-mediated apoptosis induced by Rana grylio virus infection in fish cells. Apoptosis 12, 1569–1577.

Imajoh, M, Sugiura, H., Oshima, S., 2004. Morphological changes contribute to apoptotic cell death and are affected by caspase-3 and caspase-6 inhibitors during red sea bream iridovirus permissive replication. Virology 322, 220–230.

Laliberte, J.P., Moss, B., 2009. Appraising the apoptotic mimicry model and the role of phospholipids for poxvirus entry. Proc. Natl. Acad. Sci. U. S. A. 13, 17517–17521.

Laliberte, J.P., McGinnes, L.W., Morrison, T.G., 2007. Incorporation of functional HN-F glycoprotein-containing complexes into newcastle disease virus is dependent on cholesterol and membrane lipid raft integrity. J. Virol. 81, 10636–10648.

Marsh, M., Helenius, A., 2006. Virus entry: open sesame. Cell 124, 729–740.

Martinez, G., Christian, P., Marina, C., Williams, T., 2003. Sensitivity of invertebrate iridescent virus 6 to organic solvents, detergents, enzymes and temperature treatment. Virus Res. 91, 249–254.

McSharry, J.J., Wagner, R., 1971. Lipid composition of purified vesicular stomatitis viruses. J. Virol. 7, 59–70.

Megha, London, E., 2004. Ceramide selectively displaces cholesterol from ordered lipid domains (rafts): implications for lipid raft structure and function. J. Biol. Chem. 279, 9997–10004.

Meier, C., Aricescu, A.R., Assenberg, R., Aplin, R.T., Gilbert, R.J., Grimes, J.M., Stuart, D.I., 2006. The crystal structure of ORF-9b, a lipid binding protein from the SARS coronavirus. Structure 14, 1157–1165.

Mercer, J., Helenius, A., 2008. Vaccinia virus uses macropinocytosis and apoptotic mimicry to enter host cells. Science 320, 531–535.

Merrill Jr., A.H., Sullards, M.C., Allegood, J.C., Kelly, S., Wang, E., 2005. Sphingolipidomics: high-throughput, structure-specific, and quantitative analysis of sphingolipids by liquid chromatography tandem mass spectrometry. Methods 36, 207–224.

Qiang, W, Weliky, D.P., 2009. HIV fusion peptide and its cross-linked oligomers: efficient syntheses, significance of the trimer in fusion activity, correlation of beta strand conformation with membrane cholesterol, and proximity to lipid headgroups. Biochemistry 20, 289–301.

Qin, Q.W., Lam, T.J., Sin, Y.M., Shen, H., Chang, S.F., Ngoh, G.H., Chen, C.L., 2001. Electron microscopic observations of a marine fish iridovirus isolated from brown-spotted grouper, Epinephelus tauvina. J. Virol. Methods 98, 17–24.

Reynolds, C.P., Maurer, B.J., Kolesnick, R.N., 2004. Ceramide synthesis and metabolism as a target for cancer therapy. Cancer Lett. 206, 169–180.

Roberts, K.L., Smith, G.L., 2008. Vaccinia virus morphogenesis and dissemination. Trends Microbiol. 16, 472–479.

Schlesinger, H.R., Wells, H.J., Hummeler, K., 1973. Comparison of the lipids of intracellular and extracellular rabies viruses. J. Virol. 12, 1028–1030.

Schwudke, D., Hannich, J.T., Surendranath, V., Grimard, V., Moehring, T., Burton, L., Kurzchalia, T., Shevchenko, A., 2007. Top-down lipidomic screens by multivariate analysis of high-resolution survey mass spectra. Anal. Chem. 79, 4083–4093.

Sun, Y, Kaksonen, S.C.M., Toshima, J.Y., Drubin, D.G., 2007. PtdIns (4, 5) P2 turnover is required for multiple stages during clathrin- and actin-dependent endocytic internalization. J. Cell Biol. 177, 355–367.

Song, W.J., Qin, Q.W., Qiu, J., Huang, C.H., Wang, F., Hew, C.L., 2004. Functional genomics analysis of Singapore grouper iridovirus: complete sequence determination and proteomic analysis. J. Virol. 78, 12576–12590.

Song, W.J., Lin, Q., Joshi, S.B., Lim, T.K., Hew, C.L., 2006. Proteomic studies of the Singapore grouper iridovirus. Mol. Cell. Proteomics 5, 256–264.

Thevissen, K., Francois, I.E.J., Winderickx, A.J., Pannecouque, C., Cammue, B.P.A., 2006. Ceramide involvement in apoptosis and apoptotic diseases. Mini Rev. Med. Chem. 6, 699–709.

van Meer, G., Voelker, D.R., Feigenson, C.W., 2008. Membrane lipids: where they are and how they behave. Nat. Rev. Mol. Cell Biol. 9, 112–124.

Vukelic, Z., Kalanj-Bognar, S., 2001. Cell density-dependent changes of glycosphingolipid biosynthesis in cultured human skin fibroblasts. Glycoconj. J. 18, 429–437.

Wenk, M.R., 2006. Lipidomics of host-pathogen interactions. FEBS Lett. 580, 5541–5551.

Wenk, M.R., Lucast, L., Di Paolo, G., Romanelli, A.J., Suchy, S.F., Nussbaum, R.L., Cline, G.W., Shulman, G.I., McMurray, W., De Camilli, P., 2003. Phosphoinositide profiling in complex lipid mixtures using electrospray ionization mass spectrometry. Nat. Biotechnol. 21, 813–817.

Williams, T., Thompson, P., 1995. Fatty acid profiles of invertebrate iridescent viruses. Arch. Virol. 140, 975–981.

Williams, T., Barbosa-Solomieu, V., Chinchar, V.G., 2005. A decade of advances in iridovirus research. Adv. Virus Res. 55, 173–248.

Willis, D., Granoff, A., 1974. The lipid composition of frog virus 3. Virology 61, 256–269.

Yan, X., Yu, Z., Zhang, P., Battisti, A.J., Holdaway, H.A., Chipman, P.R., Bajaj, C., Bergoin, M., Rossmann, M.G., Baker, T.S., 2009. The capsid proteins of a large, icosahedral dsDNA virus. J. Mol. Biol. 30, 1287–1299.